Glutamate weighted imaging contrast in gliomas with 7 Tesla magnetic resonance imaging

Andrew Neal[a,b,*,1], Bradford A. Moffat[c], Joel M. Stein[d], Ravi Prakash Reddy Nanga[e], Patricia Desmond[f,g], Russell T. Shinohara[h], Hari Hariharan[e], Rebecca Glarin[f,g], Katharine Drummond[i,j,k], Andrew Morokoff[i,j], Patrick Kwan[a,b,l,m], Ravinder Reddy[e], Terence J. O'Brien[a,b,l,m], Kathryn A. Davis[n]

[a] Department of Medicine, Royal Melbourne Hospital, University of Melbourne, Australia
[b] Department of Neurology, Royal Melbourne Hospital, Australia
[c] Melbourne Node of the National Imaging Facility, Department of Radiology, University of Melbourne, Australia
[d] Department of Radiology, Hospital of the University of Pennsylvania, Philadelphia, PA, United States
[e] Center for Magnetic Resonance & Optical Imaging, Department of Radiology, University of Pennsylvania, Philadelphia, PA, United States
[f] Department of Radiology, Royal Melbourne Hospital, Australia
[g] Department of Radiology and Medicine, University of Melbourne, Australia
[h] Department of Biostatistics, Epidemiology, and Informatics, Center for Clinical Epidemiology and Biostatistics, Perelman School of Medicine, University of Pennsylvania, PA, United States
[i] Department of Neurosurgery, Royal Melbourne Hospital, Australia
[j] Department of Surgery, University of Melbourne, Australia
[k] Melbourne Brain Centre, The Royal Melbourne Hospital, Australia
[l] Department of Neuroscience, Central Clinical School, Monash University, Australia
[m] Department of Neurology, The Alfred Hospital Monash University, Australia
[n] Penn Epilepsy Center, Department of Radiology, Hospital of the University of Pennsylvania, Philadelphia, PA, United States

ARTICLE INFO

ABSTRACT

Introduction: Diffuse gliomas are incurable malignancies, which undergo inevitable progression and are associated with seizure in 50–90% of cases. Glutamate has the potential to be an important glioma biomarker of survival and local epileptogenicity if it can be accurately quantified noninvasively.

Methods: We applied the glutamate-weighted imaging method GluCEST (glutamate chemical exchange saturation transfer) and single voxel MRS (magnetic resonance spectroscopy) at 7 Telsa (7 T) to patients with gliomas. GluCEST contrast and MRS metabolite concentrations were quantified within the tumour region and peritumoural rim. Clinical variables of tumour aggressiveness (prior adjuvant therapy and previous radiological progression) and epilepsy (any prior seizures, seizure in last month and drug refractory epilepsy) were correlated with respective glutamate concentrations. Images were separated into post-hoc determined patterns and clinical variables were compared across patterns.

Results: Ten adult patients with a histo-molecular (n = 9) or radiological (n = 1) diagnosis of grade II-III diffuse glioma were recruited, 40.3 +/− 12.3 years. Increased tumour GluCEST contrast was associated with prior adjuvant therapy (p = .001), and increased peritumoural GluCEST contrast was associated with both recent seizures (p = .038) and drug refractory epilepsy (p = .029). We distinguished two unique GluCEST contrast patterns with distinct clinical and radiological features. MRS glutamate correlated with GluCEST contrast within the peritumoural voxel (R = 0.89, p = .003) and a positive trend existed in the tumour voxel (R = 0.65, p = .113).

Conclusion: This study supports the role of glutamate in diffuse glioma biology. It further implicates elevated peritumoural glutamate in epileptogenesis and altered tumour glutamate homeostasis in glioma aggressiveness. Given the ability to non-invasively visualise and quantify glutamate, our findings raise the prospect of 7 T GluCEST selecting patients for individualised therapies directed at the glutamate pathway. Larger studies with prospective follow-up are required.

* Corresponding author at: Department of Neurology, Royal Melbourne Hospital, Department of Medicine, The University of Melbourne, Melbourne, Australia
  E-mail address: Andrew.neal@unimelb.edu.au (A. Neal).
[1] Present address: Department of Neuroscience, Central Clinical School, Monash University, Melbourne, Australia

1. Introduction

Diffuse gliomas account for over one third of all brain cancers (Ostrom et al., 2015) and are incurable malignancies, which undergo inevitable progression. While recent advances in molecular phenotyping can help individualise treatment(Buckner et al., 2016; Cairncross et al., 2014; van den Bent et al., 2013), there have been only incremental advances in therapeutic options in the last decade(Stupp et al., 2015). Seizures occur in approximately 50–90% of patients with diffuse gliomas over the course of their disease, with seizures more common pre-operatively and in lower grade tumours(Chang et al., 2008; Kim et al., 2013; Pallud et al., 2014a; You et al., 2012). An improved understanding of glioma biology and newer therapeutic options to improve both survival and seizure control are needed for this patient group.

There is building evidence that alterations to glutamate homeostasis in gliomas play an important role in diffuse glioma cell survival and local epileptogenicity(Buckingham et al., 2011; Campbell et al., 2012; Neal et al., 2016c; Pallud et al., 2014b; Robert et al., 2015; Ye and Sontheimer, 1999; Yuen et al., 2012). Increased extra-cellular glutamate causes excitotoxicity to peri-tumoural structures and promotes tumour invasion in pre-clinical studies(Lyons et al., 2007; Ramaswamy et al., 2014; Robert et al., 2015; Takano et al., 2001; Ye and Sontheimer, 1999). Additionally, peritumoural tissue is regarded as the region primarily responsible for epileptogenesis(Mittal et al., 2016) and increased glutamate in this tissue has been implicated in the pathobiology of glioma-associated seizures(Buckingham et al., 2011; Campbell et al., 2012; Neal et al., 2016b; Yuen et al., 2012). Glutamate therefore has the potential to be a biomarker of glioma aggressiveness and epilepsy risk. However, its utility as a biomarker relies upon the ability to accurately quantify it noninvasively.

Although Magnetic Resonance Spectroscopy (MRS) at 3 Tesla (3 T) allows the quantification of several brain molecules in glioma(Chawla et al., 2007; Liubinas et al., 2014; Rijpkema et al., 2003), the measurement of specific neurotransmitters, like glutamate is limited (Jissendi Tchofo and Baleriaux, 2009; Ramadan et al., 2013). MRS at 7 Tesla (7 T) provides an alternative to quantify tumour and peritumoural glutamate with the potential to overcome limitations at 3 T. In healthy volunteer studies, 7 T MRS offers precise detection of multiple individual metabolites, including resolution of individual glutamine and glutamate peaks(Balchandani and Naidich, 2015; Choi et al., 2010; Mekle et al., 2009). In a single 7 T study of 29 glioma patients, glutamate was elevated in the lesion compared with normal appearing white matter(Li et al., 2015). However, beyond this, there is limited literature examining glutamate measurement with 7 T MRS in brain tumours(Li et al., 2015), with no studies exploring the peritumoural region nor correlating 7 T MRS metabolites with clinical variables.

Glutamate chemical exchange saturation transfer (GluCEST) imaging, offers an alternative and potentially superior technique for high resolution non-invasive glutamate measurement in humans utilising CEST technology(Cai et al., 2012, 2013). The CEST technique relies upon a solute pool (i.e. glutamate) with exchangeable protons (e.g. amine groups) and a larger solvent pool, consisting of water. As repeated RF saturation pulses are applied at the resonant frequency of the solute, saturated solute protons exchange with unsaturated solvent protons, eventually resulting in a decrease in water signal. The difference in water signal with and without saturation at the frequency of the solute resonance can then be measured(Cai et al., 2012) as the CEST effect. There is a linear relationship between GluCEST contrast and glutamate, and GluCEST contrast has greater sensitivity for quantifying glutamate than MRS(Cai et al., 2012). Importantly, and as an additional differentiator from MRS, glutamine does not contribute to the GluCEST effect(Cai et al., 2012). To date GluCEST imaging has been used to quantify glutamate in the spinal cord of healthy volunteers(Kogan et al., 2013b), patients with mesial temporal lobe epilepsy(Davis et al., 2015) and individuals on the psychosis spectrum(Roalf et al., 2017). However, this technique has not yet been applied in those with brain tumours.

In this study, we aimed to test the feasibility of applying the magnetic resonance imaging methods GluCEST and single voxel MRS at 7 Telsa to patients with grade II-III diffuse gliomas with and without epilepsy. Within this small pilot study we also explored the following primary hypotheses: i) tumour GluCEST contrast would be increased in patients with clinical variables linked to tumour progression, ii) peritumoural GluCEST contrast would be increased in patients with clinical variables linked to epilepsy and iii) tumour and peritumoural GluCEST contrast would correlate with MRS glutamate concentration. To test this, we quantified glutamate in the tumour and peritumoural regions and correlated GluCEST contrast and MRS metabolite concentrations in corresponding regions of interest. We also distinguished distinct patterns of GluCEST contrast and correlated these patterns with clinico-pathological variables.

2. Materials and methods

2.1. Recruitment

Patients were recruited from the Royal Melbourne Hospital and Melbourne Private Hospital during 2017. Inclusion criteria were: i) 18–65 years, ii) radiological or histological diagnosis of a grade II-III supratentorial diffuse glioma. Patients were excluded if there was a contraindication to 7 T MRI.

At the time of recruitment there was limited available evidence on the safety of 7 T imaging in patients with post-craniotomy metalware in-situ, given the added potential for B0 artefact secondary to post-craniotomy metalware and the expected heterogeneity among a post-resection population, patients were excluded if they had undergone a previous craniotomy and resection. Therefore, only patients who were pre-operative or had only undergone a biopsy were included.

This study protocol was approved by the Melbourne Health Human Research and Ethics Committee (HREC 2006.199).

2.2. Clinical, pathological and radiological data collection

Clinico-pathological data were collected from medical records and patient history. WHO glioma classification was based upon the current version of the WHO classification of Tumours of the Central Nervous System(Louis et al., 2016). Additional radiological features were recorded from the 3 T clinical MRI obtained at the closest time point to 7 T MRI acquisition.

Radiological progression and the use of any adjuvant therapy between radiological diagnosis and 7 T GluCEST were used as separate surrogates for tumour progression and therefore glioma aggressiveness. Both are modified from well-established oncological treatment trial endpoints 'time to progression' and 'time to next intervention'. These were utilised given the absence of prospective follow-up from 7 T MRI.

2.3. Anti-epileptic drug use

Decisions regarding anti-epileptic drug (AED) prescription and dose adjustments were made by the patient's treating physician. Typically, patients were prescribed their first AED after either first pre-operative seizure or peri-operatively as prophylaxis. Post-operative AED dose adjustments were based on clinical response and adverse effects. AED and doses at the time of 7 T imaging were recorded.

2.4. Seizure history

Seizure history was taken by an epileptologist (AN) prior to 7 T MRI. Seizures were characterised as focal aware seizure, focal impaired awareness seizure and focal to bilateral tonic-clonic seizure(Fisher et al., 2017). Seizure frequency (seizures per month) was ascertained by retrospective patient report over the month prior to 7 T MRI. The number of seizure free months prior to 7 T MRI was also calculated; for

those without seizure this was taken from the date of presenting symptom.

Tumour Associated Epilepsy (TAE) was defined as one or more seizures attributed to a tumour. Drug resistant epilepsy was defined as failure of adequate trials of two tolerated and appropriately chosen and used AED schedules (as monotherapy or combination) to achieve sustained seizure freedom in keeping with the International League Against Epilepsy definition(Kwan et al., 2010).
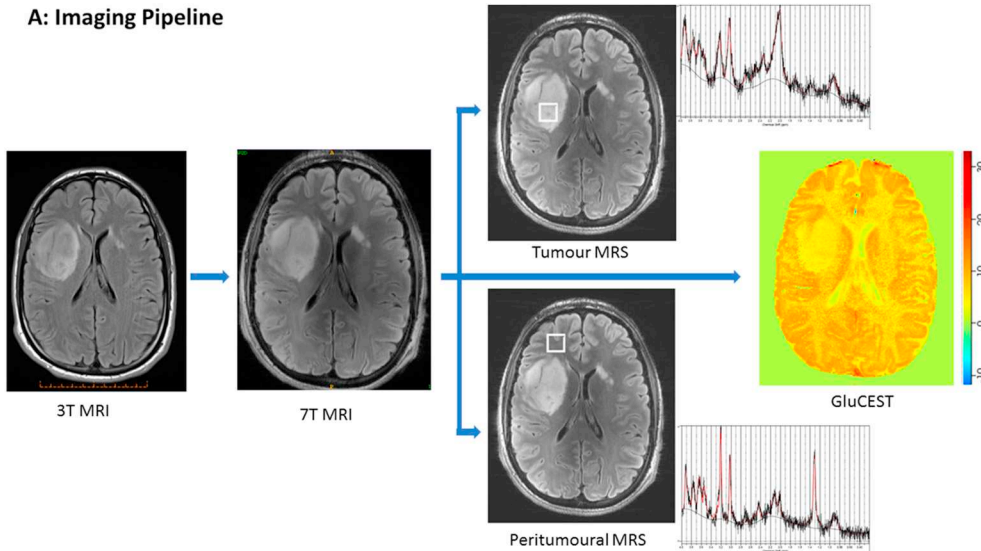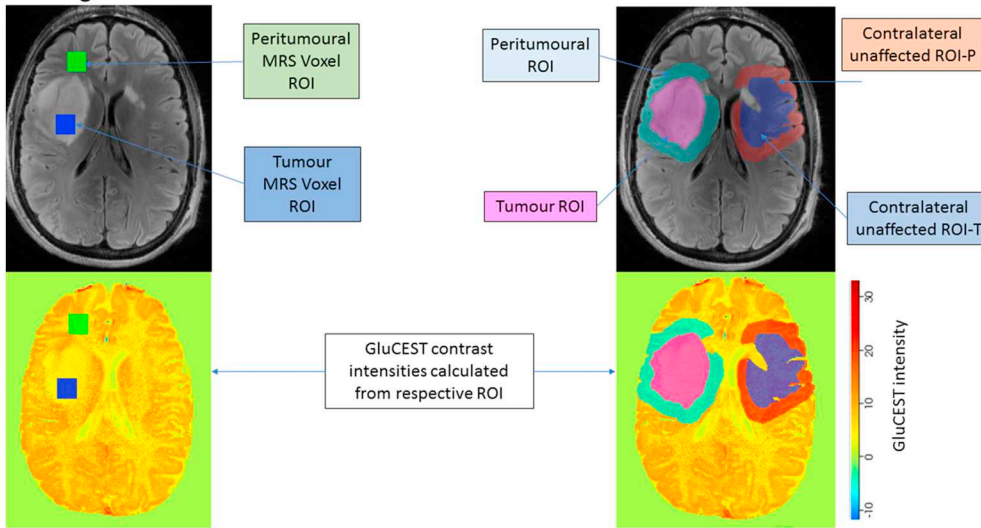

Fig. 1. 7 T imaging protocol.

Flow diagram describing imaging pipeline, regions of interest and magnetic resonant spectrum output. (A) 3 T axial image with the largest diameter of the FLAIR hyperintense lesion identified before 7 T MRI. - Corresponding 7 T axial slice (axial GluCEST acquisition slab) determined with real-time visual comparison of 3 T and 7 T MRI. 5 mm GluCEST imaging performed at the GluCEST acquisition slab location. MRS performed in tumour and peritumoural tissue with a 15mm × 15mm × 15 mm voxel within the 5 mm thick GluCEST slab. (B) Regions of interest (ROI) drawn corresponding to i) tumour MRS voxel and peritumoural MRS voxel ii) tumour, iii) 1 cm rim around tumour border (peritumoural), iv) normal appearing brain in the contralateral hemisphere approximating a mirror image of the tumour ROI (contralateral unaffected ROI-T) and v) 1 cm rim around contralateral tumour ROI (contralateral unaffected ROI-P). Note, GluCEST contrast colour scheme adjusted from standard in this figure to allow better visualisation of ROIs. (C) Example of a magnetic resonance spectrum with the individual glutamate spectrum, outlined in red, showing three glutamate distinct peaks. Cr = creatine; Glu = glutamate; -GPC = glycerophosphorylcholine; Ins = myo-inositol; NAA = *N*-acetyl aspartate; PCr = phosphocreatine.
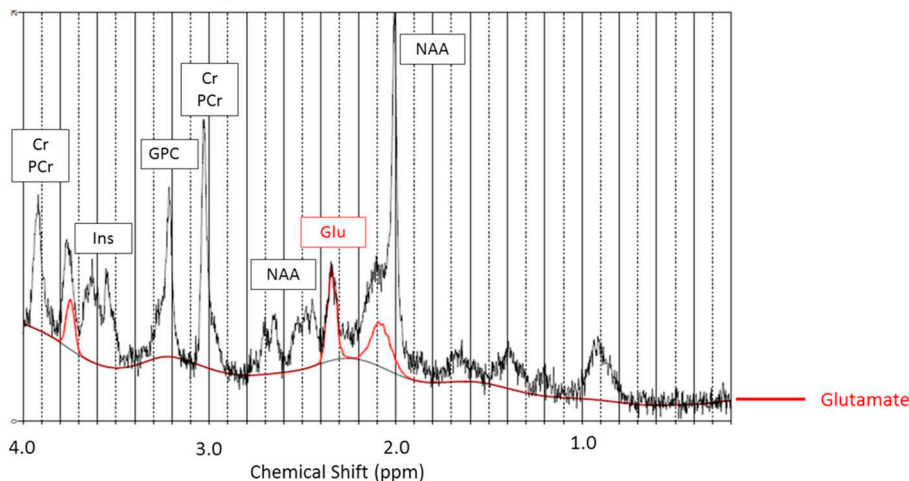
2.5. Clinico-pathological variables

Five clinico-pathological variables were derived from the extracted baseline information and imaging outcomes were compared across these outcomes: i) Tumour associated epilepsy, ii) One or more seizures in the month prior to 7 T MRI iii) Drug resistant epilepsy, iv) Radiological progression between diagnosis and 7 T MRI and v) Any prior adjuvant therapy between diagnosis and 7 T MRI.

2.6. 7 T MRI acquisition

All images were acquired on a Siemens Magnetom 7 T MRI Scanner using a 32-channel head coil optimized for parallel imaging. The imaging protocol included: i) localizer, ii) B_1 Map Sagittal 1 Slice, iii) T_1-weighted anatomical 3D magnetization prepared rapid gradient echo (MP2RAGE) images of whole brain: 192 sagittal slices, TR = 4900 ms, TE = 2.94 ms, TI = 700/2700 ms, α = 5/6°, resolution = $0.9 \times 0.9 \times 0.9$ mm^3, image matrix = 256×256, FOV = 230, Bandwidth 240 Hz/pixel, Acquisition time = 5:54 mins, iv) Partial brain T_2 axial Flair slices imaging the tumour region was performed in patients 7–10: 30 slices, TR = 9000 ms, TE = 97 ms, TI = 2600 ms, α = 135°, Slice thickness = 3 mm, resolution = 1.03 mm $\times$ 1.03 mm $\times$ 3 mm, image matrix = 180×224, FOV = 230, Bandwidth = 272 Hz/pixel, ETL = 8, Acquisition time = 2:44 mins.

Prior to 7 T MRI, the most recent standard of care 3 T MRI was reviewed with a neuroradiologist (PD). Three annotations were made corresponding to: i) axial GluCEST acquisition slab location, ii) peritumoural MRS voxel location and iii) tumoural MRS voxel location. The axial GluCEST acquisition slab location was prescribed as the axial slice with the largest diameter of the FLAIR hyperintense lesion that was outside regions expected to contribute significantly to B0 artefact, e.g. haemorrhagic tissue, surgical plates, ethmoid sinuses and base of skull.

Annotated 3 T images were also reviewed real-time and parallel to 7 T acquired images. The location of axial GluCEST acquisition slab was determined by visually comparing 3T axial, coronal and sagittal images by researchers (AN, RG, PD). For the 2D GluCEST imaging, the parameters were: slice thickness = 5 mm, flip angle = 10°, band-width = 560 Hz/pixel, in-plane resolution = 0.8×0.8 mm^2, matrix size = 208×256, GRE read out TR = 6.2 ms, TE = 3 ms, shot TR = 10,000 ms, shots per slice = 2, averages = 2, with a 800 ms long saturation pulse train (series of 96-ms Hanning windowed saturation pulses with a 4 ms inter-pulse delay (100 ms pulse train)) at B_{1rms} = 3.06μT. Raw CEST images were acquired at varying saturation offset frequencies from $\pm$ 1.8 to $\pm$ 4.2 ppm (relative to water reference) with a step-size of $\pm$ 0.3 ppm. Additionally, $\pm$ 20 and $\pm$ 100 ppm raw CEST images were also acquired. To compute the B_0 map, GRE images were collected at two echo times (TE1 = 4.24 ms; TE2 = 5.26 ms). To compute the B_1 map, two images were obtained using square preparation pulses with flip angles 30 and 60°. Total scan time for the acquisition of B_0, B_1 and CEST images were ~20 min.

MRS was performed in tumour and peritumoural tissue with a 15 mm $\times$ 15 mm $\times$ 15 mm voxel within the 5 mm thick GluCEST slab. Voxel location was determined by visually comparing the annotated 3 T axial, coronal and sagittal images by researchers (AN, RG, PD). The peritumoural MRS voxel location was chosen based upon the following criteria: i) being at the border of the T_2 FLAIR hyperintense lesion, ii) in the same plane as the axial slice with largest tumour diameter iii) including grey matter, iv) outside of brain regions expected to contribute to significant spectroscopy artefact. The tumour MRS voxel location was chosen based upon the following criteria: i) within FLAIR hyperintense lesion, ii) in the same plane as the axial slice with largest tumour diameter and if possible, iii) outside haemorrhagic or necrotic tissue. The following imaging protocol was performed: i) STEAM, TR = 8500 ms, TE = 6 ms, TM = 32 ms, α = 90°, OVS on, Only RF off = 8 averages, scan time = 1:42 mins, ii) STEAM, TR = 8500 ms,

TE = 6 ms, TM = 32 ms, α = 90°, OVS on, VAPOR Water Suppressed = 32 averages, scan time = 5:06 mins.

2.7. Imaging post-processing

2.7.1. GluCEST

CEST images obtained from $\pm$ 1.8 to $\pm$ 4.2 ppm were interpolated using the cubic spline method to generate images with a fine step-size of 0.005 ppm. B_0-corrected CEST images at $\pm$ 3 ppm were generated from the interpolated CEST images by picking signals according to the frequency shift in the B_0 map. The B_0-corrected $\pm$ 3 ppm images were then used for computing the percentage GluCEST contrast, which is equal to 100 X (($M_{-3ppm} - M_{+3ppm}$)/M_{-3ppm}), where M_{-3ppm} and M_{+3ppm} are B_0-corrected images saturated at -3 ppm and $+3$ ppm respectively, with respect to water[40]. B_1 inhomogeneity artifacts in B_0-corrected GluCEST maps were removed using B_1 calibration curves as reported(Singh et al., 2013) to get the B_0/B_1 corrected GluCEST map which was then used for further analysis.

ITK-SNAP(Yushkevich et al., 2006) software was used to co-register the post-processed axial GluCEST corrected image to the axial FLAIR. FLAIR images were re-formatted to 5 mm thick slices to align with the GluCEST slab. In 7 cases a FLAIR sequence was either not performed, or too artefact degraded and in these cases MP2RAGE T1 sequence was used. In the axial GluCEST acquisition slab plane, a region of interest (ROI) was drawn around the hyperintense lesion (FLAIR or inverted T1) by AN and independently verified by neuroradiologist PD. Inverted MP2RAGE T1 images were correlated with 3 T FLAIR to ensure an accurate tumour ROI was identified. Tumour volume was quantified with ITK-SNAP.

Within the co-registered image, ROIs were also drawn around:

i) 1 cm diameter rim around the hyperintense lesion corresponding to peritumoural tissue.
ii) Normal appearing brain in the contralateral hemisphere approximating a symmetrical mirror image of the tumour ROI. The proportion of grey/white matter involved in tumour was replicated in the contralateral hemisphere ROI. Cerebral spinal fluid (CSF) was excluded from the ROI. This ROI is defined as 'contralateral unaffected ROI-T'.
iii) 1 cm diameter rim around contralateral normal appearing brain ROI (see ii above), approximating a mirror image of the peritumoural ROI. CSF was excluded from the ROI. This ROI is defined as 'contralateral unaffected ROI-P'.
iv) 15 mm $\times$ 15 mm region corresponding to peritumoural MRS voxel and
v) 15 mm $\times$ 15 mm region corresponding to tumour MRS voxel (Fig. 1).

GluCEST contrast intensity was averaged in all respective ROIs and quantified as mean % contrast intensity. As GluCEST contrast is not an absolute value, and given that GluCEST contrast and glutamate concentration is known to quantitatively vary according to lobe and between white matter, neocortex and subcortical structures (Cai et al., 2013; Roalf et al., 2017), a GluCEST contrast ratio was calculated for tumour (tumour ROI/'contralateral unaffected ROI-T') and peritumoural (peritumoural ROI/'contralateral unaffected ROI-P') regions to allow comparison of these regions between patients.

To confirm this ratio was the most appropriate GluCEST variable to use, we calculated the co-efficient of variance for percent ROI contrast intensity using three tumour and peritumoural ratios: ROI/contralateral unaffected ROI, ROI/whole brain in axial slice and ROI/contralateral hemisphere in axial slice. For tumour ROI the lowest coefficient (and therefore, least variance) was observed with ROI/contralateral unaffected ROI, supporting its selection (respective coefficients of variance 21%, 18%, 19% and 22%). For peritumoural ROI, coefficients were similar (respective coefficients of variance (8%, 9%, 8%, 8%).

2.7.2. GluCEST and gadolinium enhanced T_1 weighted images

ITK-SNAP(Yushkevich et al., 2006) software was used to co-register the post-processed axial GluCEST corrected image to the 3T T_1 weighted images with and without gadolinium contrast. A ROI was expertly drawn around tumour displaying contrast enhancement within the co-registered GluCEST acquisition slab, this was defined as 'gadolinium enhancing tumour ROI'. GluCEST contrast intensity was averaged in this ROI and given as mean % contrast intensity. A GluCEST contrast ratio was calculated by dividing this ROI by the GluCEST contrast intensity in the 'contralateral unaffected ROI-T'.

2.7.3. Qualitative GluCEST analysis

GluCEST maps were standardised for presentation in keeping with previous GluCEST manuscripts(Cai et al., 2013; Davis et al., 2015). GluCEST images for each patient were visually inspected and described qualitatively. Where possible, images were categorised into distinct patterns determined post-hoc.

2.7.4. MRS

All spectra were analysed using LCModel™(Provencher, 1993). 16 MRS metabolites of interest were examined: alanine (Ala), aspartate (Asp), creatine (Cr), phosphocreatine (PCr), gamma-aminobutyric acid (GABA), glycine (Glc), glutamine (Gln), glutamate (Glu), glycerophosphorylcholine (GPC), glutathione (GSH), phosphocholine (PCh), myo-inositol (Ins), lactate (Lac), N-acetyl-asparate (NAA).

Only spectra with Cramer-Rao lower bound (CRLB) ratios < 20% were retained for analysis. If the CRLB for a given metabolite was > 20% in > 50% of cases, this metabolite was excluded from analysis. The spectroscopic value given for each metabolite was calculated by: metabolite/Cr + PCr. Creatine was used as an internal reference given is often unchanged or only modestly decreased in astrocytomas as compared to normal brain(Liubinas et al., 2014) and PCr was included to provide total creatine normalisation. To account for a variable proportion of grey-white matter in each peritumoural voxel, the grey-white fraction was calculated using the 7T T1 structural images. This fraction was multiplied by the respective spectroscopic value to obtain the final corrected peritumoural MRS value for each metabolite.

2.8. Primary and secondary hypotheses

The three joint primary hypotheses were that: i) tumour GluCEST contrast correlates with glioma aggressiveness (prior radiology progression, prior adjuvant therapy), ii) peritumoural GluCEST contrast correlates with seizures (any glioma associated seizures, seizures within prior month and/or drug refractory seizures) and iii) GluCEST contrast correlates with MRS glutamate within tumour and peritumoural voxels. The secondary hypotheses were that i) tumour GluCEST contrast correlates with seizures, and histology (oligodendroglial vs astrocytoma), ii) peritumoural GluCEST contrast correlates with tumour aggressiveness and histology, iii) the GluCEST contrast patterns are associated with clinical variables, iv) MRS metabolites (other than glutamate) correlate with GluCEST contrast within tumour and peritumoural voxels, and v) GluCEST contrast within tumour and peritumoural ROIs are greater than the respective contralateral unaffected ROI.

2.9. Data analysis and availability

2.9.1. Statistical analysis

A Kolmogorov-Smirnov Test was performed to test if continuous variables were normally distributed. Paired T-Tests compared GluCEST contrast between ipsilateral ROI and corresponding contralateral unaffected ROI for both tumour and peritumoural regions. Independent t-tests compared the means of GluCEST contrast intensity ratios with the chosen five clinico-pathological variables. GluCEST contrast intensity from tumour and peritumoural voxels were correlated with respective MRS metabolite concentrations with Pearson's correlation. Fisher's exact test was utilised to analyse the relationship between the five clinico-pathological endpoints and the GluCEST contrast patterns. Normally distributed continuous variables are presented as mean $+/-$ SD, while non-parametric continuous variables are presented as median [interquartile range (IQR)]. A p value of < 0.05 was chosen to represent a significant result for the investigation of primary hypotheses. For all secondary hypotheses, Bonferroni-corrected p-values were used to adjust for multiple comparisons (Supplementary Table 1). All statistical analyses were performed with SPSS - version 24 (SPSS Inc., Chicago, IL).

2.9.2. Data availability

The deidentified dataset, including all MRS and GluCEST ROI values will be shared following reasonable request from any qualified investigator.

3. Results

3.1. Baseline characteristics of the participants

Ten patients with supratentorial diffuse gliomas were recruited for the study. Baseline characteristics of the patients are described in Table 1. Individual patient characteristics are provided in supplementary material (Supplementary Table 2). 3 T and 7T images for each patient within the axial GluCEST plane including all ROIs are presented in the supplementary figures (Supplementary Fig. 1). All patients had a radiological diagnosis of diffuse glioma. Nine had a histological diagnosis of diffuse glioma; one participant had not undergone an operation at the completion of the study.

Seizure was the most common presenting symptom occurring in 70% of patients. The tumour was discovered incidentally in 2 patients and following presyncope in 1 patient. The mean number of seizures in the month preceding 7 T MRI was 4.0 [range 0–30]. There was a median of 22 days [IQR 5.5–321.5 days] between 7 T MRI and either last seizure or diagnosis. Only two patients had seizures within 24 h of 7 T and both experienced brief focal seizures with retained awareness. All patients had received a standard of care 3 T MRI prior to 7 T imaging, with a median of 2.0 months [IQR 1.1–4.8] between MRIs. The presence of tumour associated epilepsy, seizures within the month prior to 7 T and drug resistant epilepsy were all not associated with tumour volume (p = .607, p = .712, p = .430 respectively).

Four patients had received adjuvant treatment between diagnosis and 7 T MRI, with only one participant having current treatment (temozolamide) at the time of imaging. Two patients were receiving the antiepileptic drug, perampanel, an AMPA glutamate receptor antagonist, at the time of 7 T MRI.

3.1.1. Baseline imaging meta-data

The mean total scan time was 1 h 15 min (range 1 h 6 min – 1 h 34 min). Mean GluCEST scan time was 24 min (range 22 min – 33 min) and mean MRS scan time was 21 min (range 15 min – 42 min). All 10 patients tolerated the protocol and no scans needed to be aborted. MRS was too artefact degraded in one participant to be analysed (patient 1) and for technical reasons regarding data acquisition GluCEST post-processing was not successful in one patient with biopsy-related calvarial metal clips leading to artefact on B0 maps (patient 10; Supplementary Fig. 2). Therefore 9 GluCEST and MRS datasets were available for analysis.

A total of 14 MRS metabolites were analysed in each tumour and peritumoural voxel in 9 patients, resulting in 252 metabolite results. Of these, 223 results (88.5%) of results met our prespecified Cramer-Rao lower bound (CRLB) criteria to be analysed. For glutamate, 9/9 (100%) peritumoural glutamate MRS results and 8/9 (88.9%) tumour glutamate MRS results met criteria to be analysed.

Table 1

Baseline characteristics.

Variable	n (%)
Sex (female)	1 (10.0)
Age at presenting symptom	35.8 +/− 8.4 years
Age at 7T imaging	38.8 +/− 8.0 years
Biopsy	
− Before 7T MRI	6 (60.0)
− Following 7T MRI	3 (30.0)
− No operation	1 (10.0)
WHO histo-molecular classification	
− Diffuse astrocytoma IDH-mutant	4 (40.0)
− Diffuse astrocytoma IDH wildtype	1 (10.0)
− Oligodendroglioma IDH-mutant, 1p/19q co-deleted	3 (30.0)
− Anaplastic oligodendroglioma IDH-mutant, 1p/19q codeleted	1 (10.0)
− No operation performed	1 (10.0)
Side of tumour	
− Left	4 (40.0)
− Right	6 (60.0)
Location	
− Frontal	1 (10.0)
− Fronto-parietal	4 (40.0)
− Fronto-temporal	3 (30.0)
− Parieto-occipital	2 (20.0)
First symptom to 7T MRI (months)	10.6 [6.8–77.1]
Any tumour associated seizure	8 (80.0)
Seizure types (% of patients with each seizure type)	
− FAS	5 (50.0)
− FIAS	5 (50.0)
− FBTCS	4 (40.0)
Seizure free in month prior to 7T MRI	4 (40.0)
AED therapy at GluCEST	8 (80.0)
No of prior AED	
− 0	2 (20.0)
− 1	5 (50.0)
− 3+	3 (30.0)
Radiology tumour progression (Dx to 7T MRI)	6 (60.0)
Drug resistant epilepsy	2 (20.0)
Prior radiotherapy	3 (30.0)
Prior chemotherapy	3 (30.0)
Any adjuvant treatment	4 (40.0)

Abbreviations: IDH = isocitrate dehydrogenase; FAS = focal aware seizure; FIAS = focal impaired awareness seizure; FBTCS = focal to bilateral tonic-clonic seizure; Dx = diagnosis; MRI = magnetic resonance imaging.

3.2. GluCEST contrast is associated with clinical glioma phenotypes

The GluCEST contrast tumour ratio was 0.92 +/− 0.17 (range 0.66–1.16) and GluCEST contrast peritumoural ratio 0.99 +/− 0.09 (range 0.88–1.12) The wide range of ratios indicating that GluCEST contrast intensities were not consistent across the sample (see Section 3.2.4).

GluCEST contrast both within and around the tumour was compared across the 5 clinicopathological variables (Tables 2 and 3). Tumour GluCEST contrast was significantly higher in patients who had received prior adjuvant therapy between diagnosis and 7 T MRI (p = .001). The median time to adjuvant therapy in these patients was 18 months [IQR 5–41 months].

Peritumoural GluCEST contrast was significantly higher in patients who had at least one seizure in the month prior to 7 T MRI as compared to those seizure free in the prior month (p < .04) and was higher in those with drug resistant epilepsy (p < .03).

GluCEST contrast was compared between patients with an oligodendroglial histology (n = 3) and those with astrocytoma (n = 4). Tumour GluCEST contrast was higher in patients with oligodendroglial histology (1.2 +/− 0.5 vs 0.85 +/− 0.1, corrected p value = .048). Peritumoural GluCEST contrast did not differ based on histology (corrected p value ≥.99). There were insufficient IDH wildtype tumours (n = 1) for an analysis based upon IDH status.

3.3. GluCEST contrast correlates with gadolinium enhancing tumour

One patient with a radiological diagnosis of diffuse glioma had definite gadolinium enhancing tumour on co-registered 3 T-T1 weighted imaging within the axial GluCEST acquisition slab (Fig. 2). GluCEST contrast intensity ratio of the contrast enhancing tumour ROI was 1.89. Qualitatively, gadolinium enhancing tumour overlapped with regions of increased GluCEST contrast. However, the area of increased GluCEST appeared to extend beyond that which contrast enhanced and even into the peritumoural region.

3.4. GluCEST contrast correlates with peritumoural MRS glutamate

Within the tumour and peritumoural voxels, GluCEST contrast intensities were correlated with MRS metabolite concentrations (Supplementary Table 3). All 8 patients with both MRS and GluCEST data were included in this analysis. There was a significant positive correlation in the peritumoural voxel between MRS glutamate and GluCEST contrast (R = 0.89, p = .003) and a positive trend in the tumour voxel (R = 0.65, p = .113). There were no significant correlations between all other MRS metabolites and GluCEST within tumour and peritumoural voxels.

3.5. Patterns of GluCEST are associated with distinct clinical and radiological features

Following the review of clinical and imaging data, two distinct GluCEST patterns emerged within the cohort: i) tumours with relatively homogenous low GluCEST contrast and ii) tumours with heterogenous regions of elevated GluCEST contrast.

3.5.1. Diffuse gliomas with low GluCEST contrast

Four patients (patients 2, 3, 8, 9) had GluCEST imaging characterised by widespread reduced GluCEST contrast (Fig. 3). Tumour GluCEST contrast was often markedly lower than most other grey and

Table 2

GluCEST contrast ratios in tumour region according to clinical variables.

Clinical variable (n = subjects with variable present/absent)	Tumour GluCEST contrast intensity ratio in patients with clinical variable[a]	Tumour GluCEST contrast intensity ratio in patients without clinical variable[a]	P value
TAE (n = 7/2)	0.95 +/− 0.19	0.83 +/− 0.10	> 0.99 [*]
Seizure in month prior to 7 T acquisition (n = 5/4)	0.94 +/− 0.16	0.91 +/− 0.20	> 0.99 [*]
DRE (n = 2/7)	1.11 +/− 0.07	0.87 +/− 0.15	0.438 [*]
Radiological Progression since Dx (n = 6/3)	0.99 +/− 0.16	0.79 +/− 0.12	0.103
Any adjuvant therapy (n = 4/5)	1.08 +/− 0.08	0.79 +/− 0.09	0.001

TAE = tumour associated epilepsy; Sz = seizure. Dx = diagnosis; DRE = drug resistant epilepsy.

[a] Ratio of GluCEST contrast intensity in tumour to 'contralateral unaffected ROI-T'.

[*] Bonferroni corrected p value.

Table 3
GluCEST contrast ratios in peritumoural region according to clinical variables.

Clinical variable (n = subjects with variable present/absent)	Peritumoural GluCEST contrast intensity ratio in patients with clinical variable[a]	Peritumoural GluCEST contrast intensity ratio in patients without clinical variable[a]	P value
TAE (n = 7/2)	1.02 +/− 0.09	0.90 +/− 0.00	0.115
Seizure in month prior to 7 T acquisition (n = 5/4)	1.04 +/− 0.75	0.93 +/− 0.06	0.038
DRE (n = 2/7)	1.07 +/− 0.00	0.97 +/− 0.09	0.029
Radiological Progression since Dx (n = 6/3)	0.98 +/− 0.08	1.02 +/− 0.11	> 0.99*
Any adjuvant therapy (n = 4/5)	1.01 +/− 0.09	0.98 +/− 0.10	> 0.99*

TAE = tumour associated epilepsy; Sz = seizure. Dx = diagnosis; DRE = drug resistant epilepsy.

[a] Ratio of GluCEST contrast intensity in peritumoural region to 'contralateral unaffected ROI-P'.
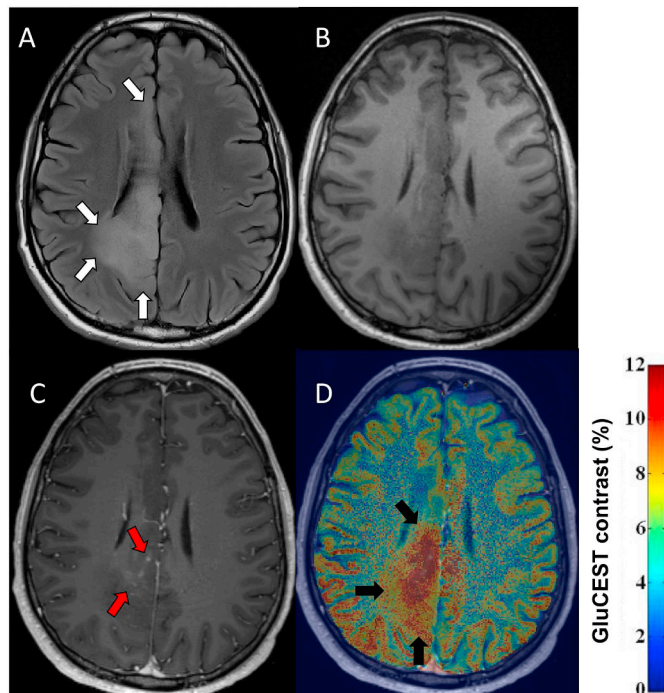
* Bonferroni corrected p value.

Fig. 2. GluCEST Contrast and gadolinium enhancing tumour.
FLAIR, T_1 weighted imaging with and without contrast and co-registered GluCEST imaging are presented for patient 4. WHO grade II oligodendroglioma IDH-mutant, 1p/19q codeleted, subsequent radiological progression and adjuvant therapy (temozolamide, radiotherapy). (A) 3 T FLAIR images in the axial GluCEST acquisition plane, tumour identified by white arrows. (B) 3 T T1 weighted images without gadolinium contrast in the axial GluCEST acquisition plane. (C) 3 T T1 weighted images with gadolinium contrast in the axial GluCEST acquisition plane with evidence of nodular, wispy mesial contrast enhancement (red arrows). (D) 3 T T1 weighted images with gadolinium co-registered with GluCEST contrast maps. Increased GluCEST contrast in a region overlapping, but extending beyond the area of gadolinium enhancement (black arrows).

white matter regions within the axial slice. Although some patients had small sutble regions of slightly increased GluCEST contrast, the predominant pattern was of reduced tumour GluCEST contrast. The GluCEST contrast tumour and peritumour ratios were 0.82 +/− 0.09 and 1.06 +/− 0.11 respectively, reflecting significantly lower GluCEST contrast in tumour compared with corresponding contralateral hemisphere ROI (p = .032) while peritumoural regions were similar between regions of interest (p = .822).

No definite regions of contrast enhancement were seen within the axial GluCEST acquisition slice location of these four patients. Of note, patient 9, who was included in this group, was the only patient in the cohort with a histological diagnosis of a grade III glioma (anaplastic oligodendroglioma IDH-mutant, 1p/19q codeleted).

3.5.2. Diffuse gliomas with heterogenous GluCEST contrast

Five patients with radiological diagnoses of diffuse glioma had heterogenous tumour GluCEST contrast (patients 1, 4, 5, 6, 7). Mean GluCEST contrast tumour and peritumoural ratios were 1.05 +/− 0.24 and 0.99 +/− 0.03 respectively. The GluCEST contrast within ipsilateral and contralateral ROIs were not significantly different within tumour (p = .474) and peritumoural (p = .654) regions.

Three patients (patients 1, 5, 6) had subtle, patchy areas of moderately increased GluCEST contrast. However, two patients (4, 7) with this heterogenous pattern, displayed striking focal regions of increased GluCEST contrast (Fig. 4). Both patients had tumours which had undergone radiological progression and had received adjuvant therapy (patient 7, chemotherapy; patient 4 radiotherapy and concurrent temozolamide).

Patient 4 had a small region of contrast enhancing tumour within the GluCEST plane, as described above (Fig. 2). Overall, across patients with this heterogenous pattern, GluCEST contrast was disproportionally increased relative to the degree (or lack thereof) of gadolinium enhancing tumour.

Case vignette. Patient 4 (Fig. 4, *E*-H) was diagnosed with a WHO grade II oligodendroglioma IDH-mutant, 1p/19q codeleted following a pre-operative seizure, 9 years prior to 7 T MRI. He developed drug resistant epilepsy and experienced a marked worsening of seizures in the setting of radiological progression. Three months prior to 7 T MRI, in the setting of further tumour progression, he was experiencing 10–15 focal motor seizures every two weeks. Perampanel, a glutamate (AMPA) receptor antagonist, was commenced and uptitrated to 6 mg daily concurrently with starting temozolamide. Following these therapy changes seizure control improved dramatically and in the subsequent 3 months he averaged one seizure per month.

3.5.3. Quantitative comparison of GluCEST contrast patterns

The five clinico-pathological variables were compared between patients with heterogenous and low GluCEST contrast patterns (Supplementary Table 4). Glioma associated epilepsy was present in 100% of heterogenous GluCEST pattern cases, and 50% with low GluCEST. Seizures in the last month were identified in 60% with a heterogenous GluCEST contrast pattern and 50% with low GluCEST contrast. Forty percent patients with heterogenous pattern met criteria for drug refractory epilepsy, although no patients did with a low GluCEST pattern. Despite the small sample size, the heterogenous pattern was associated with greater rates of radiological progression (100% vs 25%, uncorrected p = .048) and prior adjuvant therapy (80% vs 0.0% uncorrected p = .048) although these were not statistically significant after Bonferroni correction.

4. Discussion

Here, we have examined a novel 7 T molecular imaging protocol, encompassing GluCEST and MRS sequences, to quantify glutamate in
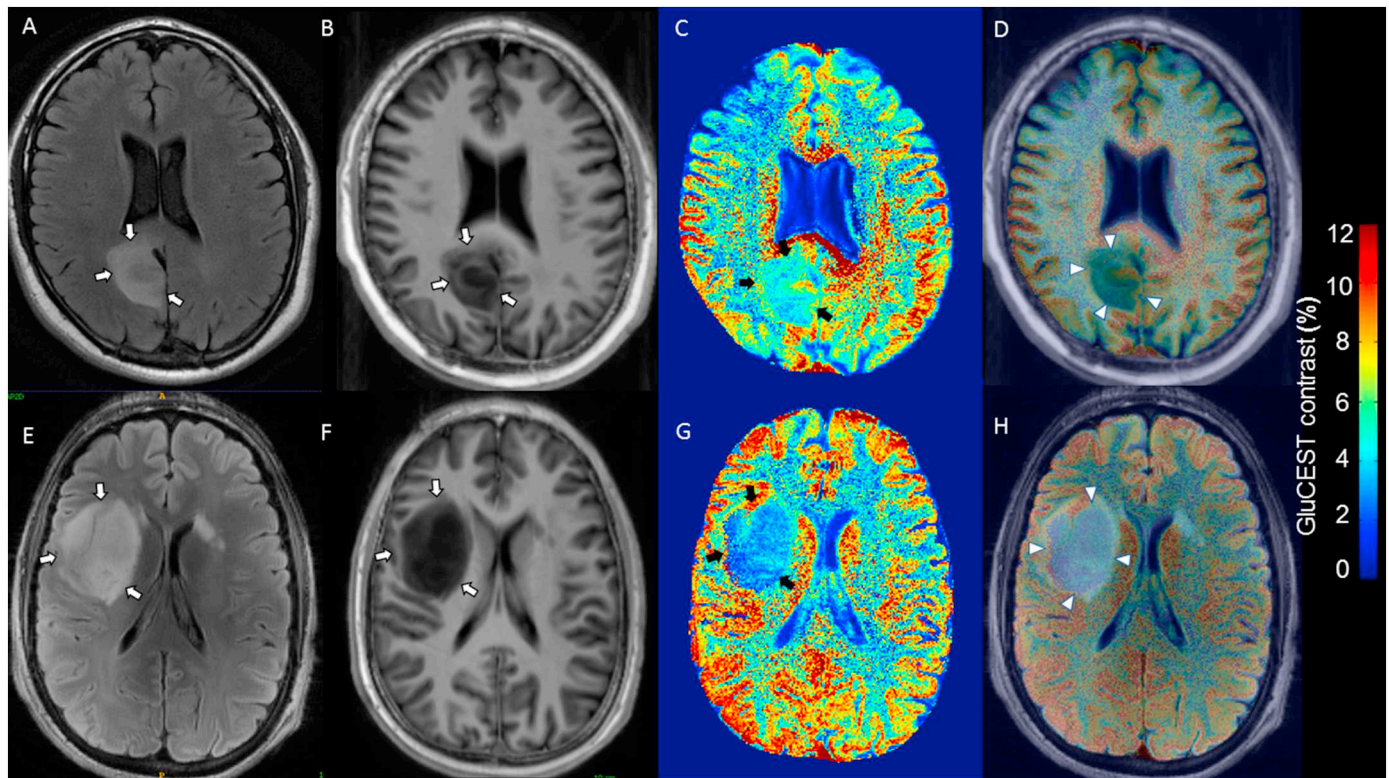
Fig. 3. Diffuse gliomas with low GluCEST contrast.

FLAIR and T$_1$ weighted images coregistered with GluCEST sequences revealing low tumour GluCEST contrast. (A–D) 37 year-old, seizure-free man with WHO grade II diffuse astrocytoma IDH-mutant (patient 3). No adjuvant therapy prior to 7 T MRI. (E–H) 30 year-old gentleman with tumour associated epilepsy, WHO grade II Diffuse astrocytoma IDH-mutant (patient 8). No adjuvant therapy prior to 7 T MRI. (A/E) = 3 T axial FLAIR (tumour identified by white arrows); (B/F) = 7 T axial T1 weighted imaging (tumour identified by white arrows); (C/G) = GluCEST contrast map (tumour identified by black arrows); (D) = Co-registered T1 and GluCEST (tumour identified by arrow heads); (H) = Co-registered FLAIR and GluCEST (tumour identified by arrow heads).

gliomas. We have shown that 7 T GluCEST imaging of gliomas is feasible and can produce high quality images permitting quantitative and qualitative assessment of molecular profiles. Secondly, we have found that increased tumour GluCEST contrast is associated with features of more aggressive diffuse gliomas, that peritumoural GluCEST contrast correlates with tumour associated seizures and we have distinguished unique GluCEST contrast patterns, with distinct clinical and radiological features.

In our analysis, increased tumour GluCEST contrast was linked to surrogates of more aggressive diffuse gliomas. Tumour GluCEST contrast was greater in those who had undergone prior adjuvant therapy and gadolinium enhancing tumour corresponded topographically with increased GluCEST contrast. Although preliminary, due to the small sample size, patients with a pattern of heterogenous increased GluCEST contrast were more likely to have undergone radiological tumour progression and to have received prior adjuvant treatment. Across our cohort, GluCEST contrast was disproportionally increased relative to gadolinium enhancement, suggesting that it may represent a more sensitive imaging biomarker of diffuse glioma aggressiveness.

Supporting our findings, adaptations to glutamate homeostasis which favour tumour cell survival are well described in gliomas. Extracellular glutamate release is increased in gliomas up to 100 fold compared with normal astrocytes(Ye and Sontheimer, 1999) (Ye et al., 1999), a process mediated primarily through SXC (system Xct) glutamate transporter upregulation(Buckingham et al., 2011; Lyons et al., 2007; Ye et al., 1999). In murine and in-vitro models, increased glioma growth and invasion have been associated with high SXC expression (Lyons et al., 2007; Robert et al., 2015) and resultant glutamate excitotoxicity(Takano et al., 2001) likely driven by glutamate receptor hyperactivation(Ramaswamy et al., 2014). Antagonism of SXC with

sulfasalazine(Chung et al., 2005; Chung and Sontheimer, 2009; Lyons et al., 2007), genetic silencing of SXC expression(Savaskan et al., 2008) and blockade of glutamate receptors(Ramaswamy et al., 2014; Ye and Sontheimer, 1999), can dramatically reduce glutamate concentrations, produce tumours with less aggressive characteristics and prolong survival in rodent models. In humans with glioma, high expression of *SLC7A11*, a gene encoding SXC, is associated with prolonged survival; a benefit postulated to be driven by reduced glutamate-mediated excitotoxicity(Robert et al., 2015).

Glutamate, however, may not be the sole driver of our tumour GluCEST signal. GluCEST contrast at 3 ppm is exquisitely sensitive to changes in pH, with a well appreciated inverse relationship with CEST signal at 3 ppm(Cai et al., 2012; Kogan et al., 2013a). Phantom GluCEST studies have shown that GluCEST increases linearly as pH decreases from 8 to 6. Extra-cellular pH within gliomas, is often acidic (6.2–6.9), while intracellular pH is typically alkaline (7.1–7.6)and low pH is felt to favour tumour growth and invasion(Coman et al., 2016; Gatenby and Gillies, 2004; Vaupel et al., 1989; Webb et al., 2011). The non-significant correlation between GluCEST and MRS tumour glutamate may reflect both the incomplete overlap of the MRS and GluCEST voxel and the potential contribution of altered pH. Without a direct tissue measurement of glutamate or acidity, the influence of pH is still in question. Taken together, the observed tumour GluCEST signal is likely a product of both pH and glutamate, as such our glutamate-weighted imaging contrast method may prove to be a more predictive biomarker of tumour aggressiveness than either component alone. On the contrary, the peritumoural may not be dominated by pH changes, explaining the significant correlation between GluCEST and MRS peritumoural glutamate. Future studies should incorporate CEST sequences that are either less sensitive to pH(Desmond and Stanisz, 2012)
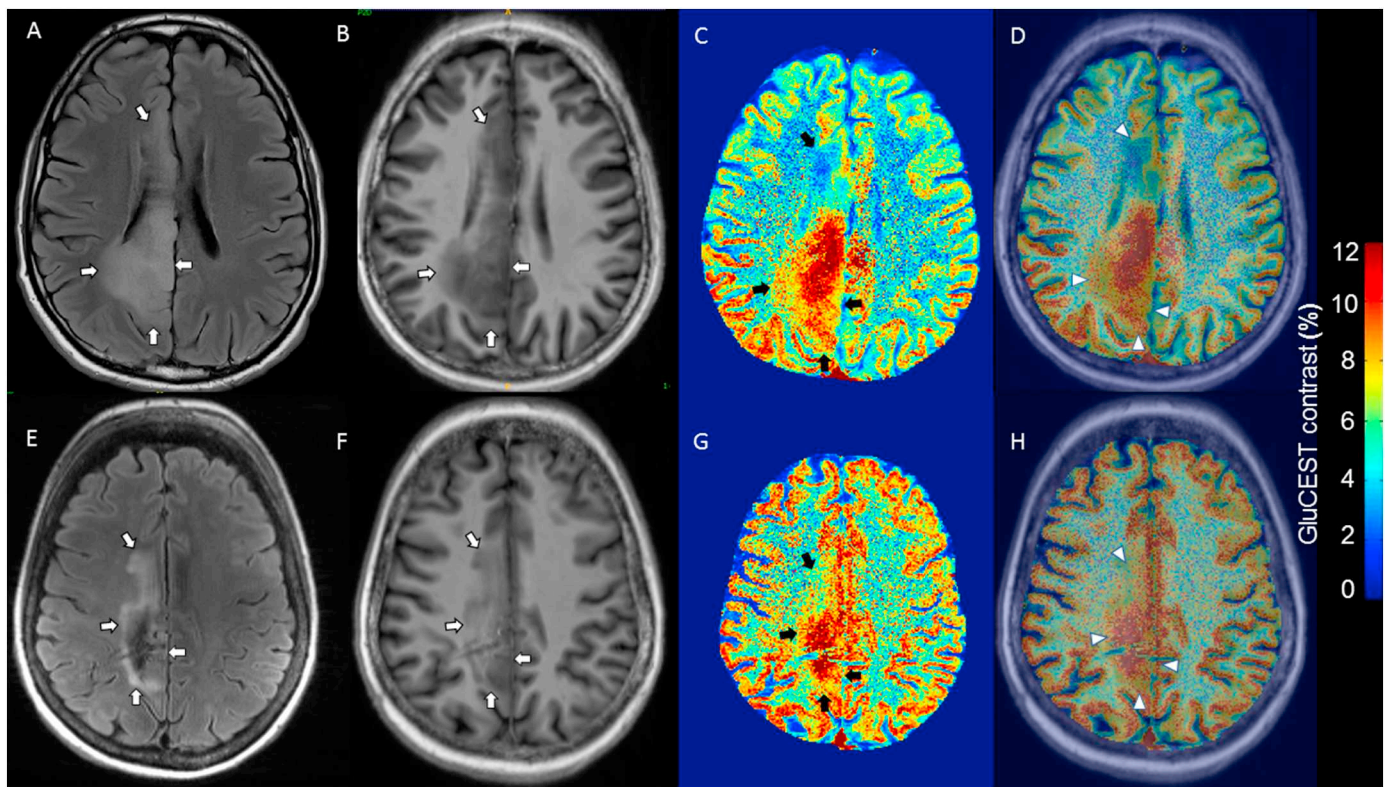
Fig. 4. Tumours with heterogenous increased GluCEST contrast.
FLAIR and T$_1$ weighted images coregistered with GluCEST sequences revealing heterogenous increased tumour GluCEST contrast. (A–D) 33 year-old male, oligo-dendroglioma IDH-mutant, 1p/19q co-deleted at diagnosis, radiological progression of tumour and treatment with chemoradiotherapy prior to 7 T MRI (patient 4). (E–H) 55 year-old woman, oligodendroglioma IDH-mutant, 1p/19q co-deleted at diagnosis, radiological progression and treatment with chemotherapy prior to 7 T MRI (patient 7). (A) = 3 T axial FLAIR (tumour identified by white arrows); (E) = 7 T axial FLAIR (tumour identified by white arrows; (B/F) = 7 T axial T1 weighted imaging (tumour identified by white arrows); (C/G) = GluCEST contrast map (tumour identified by black arrows); (D/H) = Co-registered T1 and GluCEST (tumour identified by arrow heads).

or that can assess tumour pH(Maintz et al., 2002).

The sensitivity of GluCEST for glutamate in tumour tissue has not previously been shown. We expect glutamate to be the predominant molecule contributing to the signal. Previous work has shown approximately 70% of the GluCEST signal to be derived from glutamate in normal brain, with the remaining contribution from creatine, GABA and other macromolecules(Cai et al., 2012). Theoretically these other amines which resonate at 3 ppm may also be contributing to our Glu-CEST signal, however, we expect their role to be minimal. Although creatine has been implicated in more aggressive rodent models of glioma(Cai et al., 2017), it is generally detected at relatively constant brain concentrations and frequently used as an internal control for MRS analysis. Also, GABA levels are likely to be tightly regulated and to our knowledge there is no literature supporting abnormal levels in glioma. Any additional rigid macromolecules in tumour tissue, while expected to be negligible, would compete with the GluCEST effect and under-estimate values(Cai et al., 2012). However, direct tissue quantification of these amines is required to identify the contribution of glutamate to GluCEST contrast in tumour tissue.

The correlation we have found between GluCEST contrast (which quantifies amine transfer) and more aggressive diffuse gliomas is supported by findings previously described with Amide Proton Transfer weighted (APTw) imaging(Togao et al., 2014; Zou et al., 2017). APTw is a CEST-based molecular imaging technique that can detect en-dogenous mobile amides in tissue, such as those in the cytoplasm (Bisdas et al., 2016; Zhou et al., 2003a, 2003b). APTw has been shown to distinguish tumour recurrence from radiation necrosis in rats(Zhou et al., 2011) and further studies will be required to assess if GluCEST can provide a similar role in humans. Compared with APTw, 7 T

GluCEST offers the advantage of providing a quantification an in-dividual molecular biomarker, glutamate.

Our second major finding was the association between increased peritumoural GluCEST and both drug resistant epilepsy and seizures in the month prior to 7 T imaging. These findings are consistent with a growing body of evidence implicating elevated peritumoural glutamate in the pathogenesis of tumour associated epilepsy(Buckingham et al., 2011; Campbell et al., 2012; Neal et al., 2016c; Robert et al., 2015). We did not find a similar relationship with those experiencing any previous glioma associated seizure, suggesting that peritumoural GluCEST may be a relatively dynamic biomarker of epileptogenicity and therefore seizure risk. Of note, the narrow range of peritumoural GluCEST con-trast ratios does question the ability of this method to identify subtle alterations in the peritumoural environment. Further molecular studies which optimise the identification of the epileptogenic peritumoural region are essential if these tools are to be used to guide individualised treatment decisions. There is a clear need for more precision-based therapies for tumour associated epilepsy. Poorly controlled epilepsy occurs in 10–23% of grade II-IV diffuse gliomas(Chang et al., 2008; Kerkhof et al., 2013; Pallud et al., 2014a; You et al., 2012) and the effectiveness of standard AEDs is poorer than in those with non-tumour related epilepsy(Neal et al., 2016a). Although further validation is clearly required, GluCEST offers a potential means to identify patients at high risk of seizure, and to help select those who may benefit from directed agents that target the glutamate pathway(Vecht et al., 2017).

We were able to delineate distinct patterns of GluCEST contrast among a small cohort. The heterogenous signal observed in several cases reflects the typically heterogenous pattern of tumour progression. In such tumours, quantifying glutamate with single voxel MRS or tissue

biopsy would carry a significant risk of sampling bias. The relatively homogeneous low GluCEST contrast in patients without characteristics of aggressive tumours is intriguing. GluCEST signal was often lower than normal appearing brain, suggesting a lack of mobile endogenous amine groups and it is imperative to question the validity of the glutamate signal. False negative 'glutamate' maps may be due to a very alkaline environment or even a high density of tumour cells with low water content limiting the ability to measure a change in water signal.

This was a small, proof of concept study with several important limitations. We utilised only one 5 mm axial GluCEST slice and single voxel MRS, which may not be representative of the entire tumour nor capture the most aggressive or heterogenous regions. It also introduces the problem of partial volume averaging which may have increased the degree of heterogeneity and diluted the GluCEST contrast signal. As this was not a prospectively followed cohort, we could not employ more established markers of tumour aggressiveness, eg overall survival, radiological progression or time to next intervention. Our surrogates for aggressiveness (gadolinium enhancement, previous radiological progression and prior adjuvant therapy) each have their limitations, particularly the impact of individual surgeon and patient preference on the timing of adjuvant therapy and the fact that it may be given upfront without evidence of progression. The peritumoural MRS voxel varied across patients in both location and in proportion of grey/white matter which may have influenced metabolite concentrations. An automated tumour segmentation would have provided a more robust and reproducible selection of the MRS voxels. The internal GluCEST comparison for peritumoural tissue (contralateral unaffected ROI-P) was defined based upon the 'contralateral unaffected ROI-T', therefore the proportion of grey/white tissue did not always approximate the peritumoural ROI. We narrowed our cohort to those who had only undergone a previous biopsy; further studies in post-operative patients with metalware in-situ will be required to aid in the translation of this technique to a broader patient group.

We have shown that 7 T GluCEST imaging of gliomas can produce high quality images with spatial resolution arguably superior to many existing molecular sequences. Together with the correlation with tumour aggressiveness, this novel sequence has the potential to complement existing advanced imaging techniques. However, given the ability to non-invasively visualise and quantify glutamate, our findings raise the prospect of 7 T GluCEST also being used to select patients for individualised anti-tumour and anti-seizure therapies directed at the glutamate pathway. In fact, our research groups have commenced recruitment for two phase randomised controlled trials examining perampanel in the prevention and control of glioma associated seizures (ACTRN12617000078358, ACTRN12617000073303). Patients will receive pre-operative 7 T glutamate imaging in addition to tissue analysis for measurement of tumour and peri-tumour glutamate concentrations. These trials will aim to answer an important question raised from this current study: can in-vivo imaging with GluCEST at 7 T predict survival and seizures in those with diffuse gliomas and be used to select patients for individualised tumour and seizure therapies.

Supplementary data to this article can be found online at https://doi.org/10.1016/j.nicl.2019.101694.

Funding

Declarations of interest

References

Balchandani, P., Naidich, T.P., 2015. Ultra-high-field MR neuroimaging. AJNR Am. J. Neuroradiol. 36, 1204–1215.

Bisdas, S., Chadzynski, G.L., Braun, C., Schittenhelm, J., Skardelly, M., Hagberg, G.E., Ethofer, T., Pohmann, R., Shajan, G., Engelmann, J., Tabatabai, G., Ziemann, U., Ernemann, U., Scheffler, K., 2016. MR spectroscopy for in vivo assessment of the oncometabolite 2-hydroxyglutarate and its effects on cellular metabolism in human brain gliomas at 9.4T. J. Magn. Reson. Imaging 44, 823–833.

Buckingham, S.C., Campbell, S.L., Haas, B.R., Montana, V., Robel, S., Ogunrinu, T., Sontheimer, H., 2011. Glutamate release by primary brain tumors induces epileptic activity. Nat. Med. 17, 1269–1274.

Buckner, J.C., Shaw, E.G., Pugh, S.L., Chakravarti, A., Gilbert, M.R., Barger, G.R., Coons, S., Ricci, P., Bullard, D., Brown, P.D., Stelzer, K., Brachman, D., Suh, J.H., Schultz, C.J., Bahary, J.P., Fisher, B.J., Kim, H., Murtha, A.D., Bell, E.H., Won, M., Mehta, M.P., Curran Jr., W.J., 2016. Radiation plus procarbazine, CCNU, and vincristine in low-grade glioma. N. Engl. J. Med. 374, 1344–1355.

Cai, K., Haris, M., Singh, A., Kogan, F., Greenberg, J.H., Hariharan, H., Detre, J.A., Reddy, R., 2012. Magnetic resonance imaging of glutamate. Nat. Med. 18, 302–306.

Cai, K., Singh, A., Roalf, D.R., Nanga, R.P., Haris, M., Hariharan, H., Gur, R., Reddy, R., 2013. Mapping glutamate in subcortical brain structures using high-resolution GluCEST MRI. NMR Biomed. 26, 1278–1284.

Cai, K., Tain, R.W., Zhou, X.J., Damen, F.C., Scotti, A.M., Hariharan, H., Poptani, H., Reddy, R., 2017. Creatine CEST MRI for differentiating gliomas with different degrees of aggressiveness. Mol. Imaging Biol. 19, 225–232.

Cairncross, J.G., Wang, M., Jenkins, R.B., Shaw, E.G., Giannini, C., Brachman, D.G., Buckner, J.C., Fink, K.L., Souhami, L., Laperriere, N.J., Huse, J.T., Mehta, M.P., Curran Jr., W.J., 2014. Benefit from procarbazine, lomustine, and vincristine in oligodendroglial tumors is associated with mutation of IDH. J. Clin. Oncol. 32, 783–790.

Campbell, S.L., Buckingham, S.C., Sontheimer, H., 2012. Human glioma cells induce hyperexcitability in cortical networks. Epilepsia 53, 1360–1370.

Chang, E.F., Potts, M.B., Keles, G.E., Lamborn, K.R., Chang, S.M., Barbaro, N.M., Berger, M.S., 2008. Seizure characteristics and control following resection in 332 patients with low-grade gliomas. J. Neurosurg. 108, 227–235.

Chawla, S., Wang, S., Wolf, R.L., Woo, J.H., Wang, J., O'Rourke, D.M., Judy, K.D., Grady, M.S., Melhem, E.R., Poptani, H., 2007. Arterial spin-labeling and MR spectroscopy in the differentiation of gliomas. AJNR Am. J. Neuroradiol. 28, 1683–1689.

Choi, C., Dimitrov, I.E., Douglas, D., Patel, A., Kaiser, L.G., Amezcua, C.A., Maher, E.A., 2010. Improvement of resolution for brain coupled metabolites by optimized (1)H MRS at 7T. NMR Biomed. 23, 1044–1052.

Chung, W.J., Sontheimer, H., 2009. Sulfasalazine inhibits the growth of primary brain tumors independent of nuclear factor-kappaB. J. Neurochem. 110, 182–193.

Chung, W.J., Lyons, S.A., Nelson, G.M., Hamza, H., Gladson, C.L., Gillespie, G.Y., Sontheimer, H., 2005. Inhibition of cystine uptake disrupts the growth of primary brain tumors. J. Neurosci. 25, 7101–7110.

Coman, D., Huang, Y., Rao, J.U., De Feyter, H.M., Rothman, D.L., Juchem, C., Hyder, F., 2016. Imaging the intratumoral-peritumoral extracellular pH gradient of gliomas. NMR Biomed. 29, 309–319.

Davis, K.A., Nanga, R.P., Das, S., Chen, S.H., Hadar, P.N., Pollard, J.R., Lucas, T.H., Shinohara, R.T., Litt, B., Hariharan, H., Elliott, M.A., Detre, J.A., Reddy, R., 2015. Glutamate imaging (GluCEST) lateralizes epileptic foci in nonlesional temporal lobe epilepsy. Sci. Transl. Med. 7 (309ra161).

van den Bent, M.J., Brandes, A.A., Taphoorn, M.J., Kros, J.M., Kouwenhoven, M.C., Delattre, J.Y., Bernsen, H.J., Frenay, M., Tijssen, C.C., Grisold, W., Sipos, L., Enting, R.H., French, P.J., Dinjens, W.N., Vecht, C.J., Allgeier, A., Lacombe, D., Gorlia, T., Hoang-Xuan, K., 2013. Adjuvant procarbazine, lomustine, and vincristine chemotherapy in newly diagnosed anaplastic oligodendroglioma: long-term follow-up of EORTC brain tumor group study 26951. J. Clin. Oncol. 31, 344–350.

Desmond, K.L., Stanisz, G.J., 2012. Understanding quantitative pulsed CEST in the presence of MT. Magn. Reson. Med. 67, 979–990.

Fisher, R.S., Cross, J.H., French, J.A., Higurashi, N., Hirsch, E., Jansen, F.E., Lagae, L., Moshe, S.L., Peltola, J., Roulet Perez, E., Scheffer, I.E., Zuberi, S.M., 2017. Operational classification of seizure types by the international league against epilepsy: position paper of the ILAE commission for classification and terminology. Epilepsia 58, 522–530.

Gatenby, R.A., Gillies, R.J., 2004. Why do cancers have high aerobic glycolysis? Nat. Rev. Cancer 4, 891–899.

Jissendi Tchofo, P., Baleriaux, D., 2009. Brain (1)H-MR spectroscopy in clinical neuroimaging at 3T. J. Neuroradiol. 36, 24–40.

Kerkhof, M., Dielemans, J.C., van Breemen, M.S., Zwinkels, H., Walchenbach, R., Taphoorn, M.J., Vecht, C.J., 2013. Effect of valproic acid on seizure control and on survival in patients with glioblastoma multiforme. Neuro-Oncology 15, 961–967.

Kim, Y.H., Park, C.K., Kim, T.M., Choi, S.H., Kim, Y.J., Choi, B.S., Kim, J.H., Lee, S.H., Kim, C.Y., Kim, I.A., Heo, D.S., Kim, I.H., Kim, D.G., Jung, H.W., 2013. Seizures during the management of high-grade gliomas: clinical relevance to disease progression. J. Neuro-Oncol. 113, 101–109.

Kogan, F., Hariharan, H., Reddy, R., 2013a. Chemical exchange saturation transfer (CEST) imaging: description of technique and potential clinical applications. Curr. Radiol. Rep. 1, 102–114.

Kogan, F., Singh, A., Debrosse, C., Haris, M., Cai, K., Nanga, R.P., Elliott, M., Hariharan, H., Reddy, R., 2013b. Imaging of glutamate in the spinal cord using GluCEST. NeuroImage 77, 262–267.

Kwan, P., Arzimanoglou, A., Berg, A.T., Brodie, M.J., Allen Hauser, W., Mathern, G., Moshe, S.L., Perucca, E., Wiebe, S., French, J., 2010. Definition of drug resistant epilepsy: consensus proposal by the ad hoc Task Force of the ILAE Commission on Therapeutic strategies. Epilepsia 51, 1069–1077.

Li, Y., Larson, P., Chen, A.P., Lupo, J.M., Ozhinsky, E., Kelley, D., Chang, S.M., Nelson, S.J., 2015. Short-echo three-dimensional H-1 MR spectroscopic imaging of patients with glioma at 7 Tesla for characterization of differences in metabolite levels. J. Magn. Reson. Imaging 41, 1332–1341.

Liubinas, S.V., Drummond, K.J., Desmond, P.M., Bjorksten, A., Morokoff, A.P., Kaye, A.H., O'Brien, T.J., Moffat, B.A., 2014. Glutamate quantification in patients with supratentorial gliomas using chemical shift imaging. NMR Biomed. 27, 570–577.

Louis, D.N., Perry, A., Reifenberger, G., von Deimling, A., Figarella-Branger, D., Cavenee, W.K., Ohgaki, H., Wiestler, O.D., Kleihues, P., Ellison, D.W., 2016. The 2016 world health organization classification of tumors of the central nervous system: a summary. Acta Neuropathol. 131, 803–820.

Lyons, S.A., Chung, W.J., Weaver, A.K., Ogunrinu, T., Sontheimer, H., 2007. Autocrine glutamate signaling promotes glioma cell invasion. Cancer Res. 67, 9463–9471.

Maintz, D., Heindel, W., Kugel, H., Jaeger, R., Lackner, K.J., 2002. Phosphorus-31 MR spectroscopy of normal adult human brain and brain tumours. NMR Biomed. 15, 18–27.

Mekle, R., Mlynarik, V., Gambarota, G., Hergt, M., Krueger, G., Gruetter, R., 2009. MR spectroscopy of the human brain with enhanced signal intensity at ultrashort echo times on a clinical platform at 3T and 7T. Magn. Reson. Med. 61, 1279–1285.

Mittal, S., Barkmeier, D., Hua, J., Pai, D.S., Fuerst, D., Basha, M., Loeb, J.A., Shah, A.K., 2016. Intracranial EEG analysis in tumor-related epilepsy: evidence of distant epileptic abnormalities. Clin. Neurophysiol. 127, 238–244.

Neal, A., Morokoff, A., O'Brien, T.J., Kwan, P., 2016a. Postoperative seizure control in patients with tumor-associated epilepsy. Epilepsia 57, 1779–1788.

Neal, A., Yuen, T., Bjorksten, A.R., Kwan, P., O'Brien, T.J., Morokoff, A., 2016b. Peritumoural glutamate correlates with post-operative seizures in supratentorial gliomas. J. Neuro-Oncol. 129, 259–267.

Neal, A., Yuen, T., Bjorksten, A.R., Kwan, P., O'Brien, T.J., Morokoff, A., 2016c. Peritumoural glutamate correlates with post-operative seizures in supratentorial gliomas. J. Neuro-Oncol.

Ostrom, Q.T., Gittleman, H., Fulop, J., Liu, M., Blanda, R., Kromer, C., Wolinsky, Y., Kruchko, C., Barnholtz-Sloan, J.S., 2015. CBTRUS statistical report: primary brain and central nervous system tumors diagnosed in the UNITED STATES in 2008–2012. Neuro-Oncology 17 (Suppl. 4), iv1–iv62.

Pallud, J., Audureau, E., Blonski, M., Sanai, N., Bauchet, L., Fontaine, D., Mandonnet, E., Dezamis, E., Psimaras, D., Guyotat, J., Peruzzi, P., Page, P., Gal, B., Parraga, E., Baron, M.H., Vlaicu, M., Guillevin, R., Devaux, B., Duffau, H., Taillandier, L., Capelle, L., Huberfeld, G., 2014a. Epileptic seizures in diffuse low-grade gliomas in adults. Brain 137, 449–462.

Pallud, J., Le Van Quyen, M., Bielle, F., Pellegrino, C., Varlet, P., Labussiere, M., Cresto, N., Dieme, M.J., Baulac, M., Duyckaerts, C., Kourdougli, N., Chazal, G., Devaux, B., Rivera, C., Miles, R., Capelle, L., Huberfeld, G., 2014b. Cortical GABAergic excitation contributes to epileptic activities around human glioma. Sci. Transl. Med. 6, 244ra289.

Provencher, S.W., 1993. Estimation of metabolite concentrations from localized in vivo proton NMR spectra. Magn. Reson. Med. 30, 672–679.

Ramadan, S., Lin, A., Stanwell, P., 2013. Glutamate and glutamine: a review of in vivo MRS in the human brain. NMR Biomed. 26, 1630–1646.

Ramaswamy, P., Aditi Devi, N., Hurmath Fathima, K., Dalavaikodihalli Nanjaiah, N., 2014. Activation of NMDA receptor of glutamate influences MMP-2 activity and proliferation of glioma cells. Neurol. Sci. 35, 823–829.

Rijpkema, M., Schuuring, J., van der Meulen, Y., van der Graaf, M., Bernsen, H., Boerman, R., van der Kogel, A., Heerschap, A., 2003. Characterization of oligodendrogliomas using short echo time 1H MR spectroscopic imaging. NMR Biomed. 16, 12–18.

Roalf, D.R., Nanga, R.P., Rupert, P.E., Hariharan, H., Quarmley, M., Calkins, M.E., Dress, E., Prabhakaran, K., Elliott, M.A., Moberg, P.J., Gur, R.C., Gur, R.E., Reddy, R., Turetsky, B.I., 2017. Glutamate imaging (GluCEST) reveals lower brain GluCEST contrast in patients on the psychosis spectrum. Mol. Psychiatry 22, 1298–1305.

Robert, S.M., Buckingham, S.C., Campbell, S.L., Robel, S., Holt, K.T., Ogunrinu-Babarinde, T., Warren, P.P., White, D.M., Reid, M.A., Eschbacher, J.M., Berens, M.E., Lahti, A.C., Nabors, L.B., Sontheimer, H., 2015. SLC7A11 expression is associated with seizures and predicts poor survival in patients with malignant glioma. Sci. Transl. Med. 7 (289ra286).

Savaskan, N.E., Heckel, A., Hahnen, E., Engelhorn, T., Doerfler, A., Ganslandt, O., Nimsky, C., Buchfelder, M., Eyupoglu, I.Y., 2008. Small interfering RNA-mediated xCT silencing in gliomas inhibits neurodegeneration and alleviates brain edema. Nat. Med. 14, 629–632.

Singh, A., Cai, K., Haris, M., Hariharan, H., Reddy, R., 2013. On B1 inhomogeneity correction of in vivo human brain glutamate chemical exchange saturation transfer contrast at 7T. Magn. Reson. Med. 69, 818–824.

Stupp, R., Taillibert, S., Kanner, A.A., Kesari, S., Steinberg, D.M., Toms, S.A., Taylor, L.P., Lieberman, F., Silvani, A., Fink, K.L., Barnett, G.H., Zhu, J.J., Henson, J.W., Engelhard, H.H., Chen, T.C., Tran, D.D., Sroubek, J., Tran, N.D., Hottinger, A.F., Landolfi, J., Desai, R., Caroli, M., Kew, Y., Honnorat, J., Idbaih, A., Kirson, E.D., Weinberg, U., Palti, Y., Hegi, M.E., Ram, Z., 2015. Maintenance therapy with tumor-treating fields plus temozolomide vs temozolomide alone for glioblastoma: a randomized clinical trial. JAMA 314, 2535–2543.

Takano, T., Lin, J.H., Arcuino, G., Gao, Q., Yang, J., Nedergaard, M., 2001. Glutamate release promotes growth of malignant gliomas. Nat. Med. 7, 1010–1015.

Togao, O., Yoshiura, T., Keupp, J., Hiwatashi, A., Yamashita, K., Kikuchi, K., Suzuki, Y., Suzuki, S.O., Iwaki, T., Hata, N., Mizoguchi, M., Yoshimoto, K., Sagiyama, K., Takahashi, M., Honda, H., 2014. Amide proton transfer imaging of adult diffuse gliomas: correlation with histopathological grades. Neuro-Oncology 16, 441–448.

Vaupel, P., Kallinowski, F., Okunieff, P., 1989. Blood flow, oxygen and nutrient supply, and metabolic microenvironment of human tumors: a review. Cancer Res. 49, 6449–6465.

Vecht, C., Duran-Pena, A., Houillier, C., Durand, T., Capelle, L., Huberfeld, G., 2017. Seizure response to perampanel in drug-resistant epilepsy with gliomas: early observations. J. Neuro-Oncol. 133, 603–607.

Webb, B.A., Chimenti, M., Jacobson, M.P., Barber, D.L., 2011. Dysregulated pH: a perfect storm for cancer progression. Nat. Rev. Cancer 11, 671–677.

Ye, Z.C., Sontheimer, H., 1999. Glioma cells release excitotoxic concentrations of glutamate. Cancer Res. 59, 4383–4391.

Ye, Z.C., Rothstein, J.D., Sontheimer, H., 1999. Compromised glutamate transport in human glioma cells: reduction-mislocalization of sodium-dependent glutamate transporters and enhanced activity of cystine-glutamate exchange. J. Neurosci. 19, 10767–10777.

You, G., Sha, Z.Y., Yan, W., Zhang, W., Wang, Y.Z., Li, S.W., Sang, L., Wang, Z., Li, G.L., Li, S.W., Song, Y.J., Kang, C.S., Jiang, T., 2012. Seizure characteristics and outcomes in 508 Chinese adult patients undergoing primary resection of low-grade gliomas: a clinicopathological study. Neuro-Oncology 14, 230–241.

Yuen, T.I., Morokoff, A.P., Bjorksten, A., D'Abaco, G., Paradiso, L., Finch, S., Wong, D., Reid, C.A., Powell, K.L., Drummond, K.J., Rosenthal, M.A., Kaye, A.H., O'Brien, T.J., 2012. Glutamate is associated with a higher risk of seizures in patients with gliomas. Neurology 79, 883–889.

Yushkevich, P.A., Piven, J., Hazlett, H.C., Smith, R.G., Ho, S., Gee, J.C., Gerig, G., 2006. User-guided 3D active contour segmentation of anatomical structures: significantly improved efficiency and reliability. NeuroImage 31, 1116–1128.

Zhou, J., Lal, B., Wilson, D.A., Laterra, J., van Zijl, P.C., 2003a. Amide proton transfer (APT) contrast for imaging of brain tumors. Magn. Reson. Med. 50, 1120–1126.

Zhou, J., Payen, J.F., Wilson, D.A., Traystman, R.J., van Zijl, P.C., 2003b. Using the amide proton signals of intracellular proteins and peptides to detect pH effects in MRI. Nat. Med. 9, 1085–1090.

Zhou, J., Tryggestad, E., Wen, Z., Lal, B., Zhou, T., Grossman, R., Wang, S., Yan, K., Fu, D.X., Ford, E., Tyler, B., Blakeley, J., Laterra, J., van Zijl, P.C., 2011. Differentiation between glioma and radiation necrosis using molecular magnetic resonance imaging of endogenous proteins and peptides. Nat. Med. 17, 130–134.

Zou, T., Yu, H., Jiang, C., Wang, X., Jiang, S., Rui, Q., Mei, Y., Zhou, J., Wen, Z., 2017. Differentiating the histologic grades of gliomas preoperatively using amide proton transfer-weighted (APTW) and intravoxel incoherent motion MRI. NMR Biomed. 31 e3850.